P2

NASA TECHNICAL MEMORANDUM

NASA TM X-62,312

ARTIFICIAL METEOR ABLATION STUDIES: OLIVINE

Maxwell B. Blanchard

Ames Research Center
Moffett Field, Calif. 94035

and

Gary G. Cunningham

California State University
San Jose, Calif. 95132

October 1973

Artificial Meteor Ablation Studies: Olivine

Maxwell B. Blanchard

Space Science Division, Ames Research Center, NASA
Moffett Field, California 94035

Gary G. Cunningham

Geology Department, California State University
San Jose, California 95132

ABSTRACT

Artificial meteor ablation has been performed on a Mg-rich olivine sample using an arc-heated plasma of ionized air. Experimental conditions simulated a meteor traveling about 12 km/sec at an altitude of 70 km. The mineral content of the original olivine sample was 98% olivine (including traces of olivine alteration products) and 2% chromite. Forsterite content of the original olivine was Fo-89. After ablation, the forsterite content had increased to Fo-94 in the recrystallized olivine. In addition, lamella-like intergrowths of magnetite were prevalent constituents. Wherever magnetite occurred, there was an increase in Mg and a corresponding decrease in Fe for the recrystallized olivine. The Fe for the magnetite exsolved from the original olivine crystals. Individual particles (i.e., spherules) were also characterized by magnetite intergrowths. Fusion crusts on the Allende and Murchison meteorites were compared with the fusion crust on the olivine sample. The Allende fusion crust consisted of a recrystallized olivine, which was more Mg-rich and Fe-deficient than the original meteorite's olivine, and abundant magnetite grains. Although troilite and pentlandite were the common opaque mineral constituents in this meteorite, magnetite was the principal opaque mineral found in the fusion crust. The Murchison meteorite revealed similar magnetite grains in a recrystallized olivine, even though the original meteorite had principally a chamosite matrix. The similarity between the fusion crusts produced by real ablation and the fusion crust produced by artificial ablation proves the simulation is valid. The observed textural and mineralogical features can be used as criteria for identifying ablation debris on the earth and in the atmosphere.

Much of the meteoritic material reaching the earth is ablation debris. This debris has sometimes been misidentified as cosmic dust. *Kornblum* [1969] has clearly shown the only true (unaltered) cosmic dust that could possibly reach the earth's surface would have to be no larger than a few microns in size. There are several methods to collect meteor ablation debris for analysis. *Finkleman* [1972] has correctly identified ablation debris in deep sea manganese nodules. Atmospheric collections have been made with high altitude aircraft [*Carr*, 1970] and long-residence-time, high altitude balloons [*Brownlee and Hodge*, 1969]. All of the collections have always contained terrestrial contaminants. Distinguishing between contaminants and the meteor ablation debris has been difficult.

Because facilities have recently become available which can reliably duplicate the ablation environment, it has been possible to study the ablation process and analyze the ablation debris to develop proper identification criteria. A systematic study [*Blanchard*, 1969] was initiated to gain better understanding of the ablation process and to develop identification criteria for ablation products. Carefully analyzed mineral samples were ablated by simulating a meteor entering the earth's atmosphere. Initial studies with iron oxides [*Blanchard*, 1970a, b, and 1972] produced the following criteria as indicative of ablation debris in general. The shape of material larger than 1 mm exhibits features characteristic of melt products (i.e., spherules, droplets, and stringers). However, a substantial portion of the material smaller than 1 mm shows no signs of ever having been melted (i.e., subangular grains). The texture of the debris exhibits myrmekitic-like intergrowths of new phases in all melt products. Mineralogically, new minerals are formed at the expense of original ones. One such mineral (wustite) is metastable and is formed by a reducing environment. Quenching conditions are responsible for its preservation. Glasses are formed as myrmekitic-like intergrowths in the melt products. Solid-state mineral transformations

occur in the fusion crust. Finally, volatile elements (i.e., P and Cl) are depleted. Some were observed to have been depleted by about 50% of their original content.

The objective of this paper is to add to the previous criteria by analyzing a sample more representative of meteoritic material, yet simple enough to prevent analytical complications. Olivine was chosen because it is a common meteoritic mineral. Preliminary results of these olivine studies have been reported by *Blanchard and Cunningham* [1973].

PROCEDURE

A constricted-arc supersonic jet was used for the ablation simulations. Details of the facility's design and performance characteristics have been reported by *Shepard et al.* [1967]. For this experiment, the conditions simulated a low velocity meteor traveling about 12 km/sec at an altitude of about 70 km. Ablation occurs when the olivine sample is introduced to the flowing plasma beam. The beam consists mostly of air and electrons. The ablation period lasts for about 30 sec, after which time the sample has been consumed. The oxygen partial pressure in the plasma upstream of the sample during ablation is about 0.2 mm. This may become as high as 12 mm in the gas cap along the sample's front face.

The olivine sample was cut into a cube, 4 cm on a side, with a small hole in one side for mounting. It was dried at 80°C for 24 hr to remove water. The sample was mounted on a movable copper stang in a vacuum chamber, about 8 cm from the nozzle (Figure 1) through which the plasma entered. Debris for analysis came from the following two main sources: (1) the flanges, stringers, and fusion crust along the sample's front face; and (2) the individual particles (i.e., spherules) recovered from a copper collecting plate located downstream of the ablating sample.

Analytical studies were conducted on the olivine sample, fusion crust (ablation zone on original sample), and ablated debris to characterize the morphological, textural, elemental, and mineralogical changes. Constituent minerals were identified by optical microscopy and X-ray diffraction. Mineral elemental composition was determined with the electron microprobe. Submicron-sized features were studied by scanning electron microscopy. Bulk elemental analyses were performed by wet chemistry. Petrographic thin sections and polished sections of the sample, fusion crust, and ablated debris were used to compare observed results with previous studies and two meteorite fusion crusts. Ablated particles were divided into groups based on their morphology. These groups were used to select representative samples for X-ray diffraction and microprobe studies.

The minerals present in the original and ablated samples were identified by X-ray diffraction. The olivine composition was determined using the methods of both *Yoder and Sahama* [1957], and *Hotz and Jackson* [1963]. The accessory mineral chromite was obtained by crushing the olivine sample and concentrating it using density separation with methylene iodide (ρ = 3.2 gm/cm^3). The magnetite intergrowths ($<10\,\mu$) were concentrated from the ablated olivine by fine grinding and subsequent electromagnetic separation. Ablated single particles were identified using Debye-Scherrer powder diffraction techniques. Individual particles ($<300\,\mu$) were mounted on glass fibers with Apiezon grease, then positioned in chucks and placed in 57.3-mm-diameter Debye-Scherrer cameras. Apiezon grease and pure silica fibers were used because they produced no interfering diffraction patterns even after long (24 hr) exposures. The X-ray scatter from the air was reduced during these long exposure times by continuously purging the cameras with He. The X-rays from a Cr target (λ = 2.291 Å) were used to eliminate secondary fluorescence from Cr and Fe in the samples. Many of these small particles produced spotty and/or incomplete diffraction patterns. These patterns made film measuring tedious and

time-consuming. To improve identifications, a film overlay technique was used. With this method, diffraction patterns of all minerals expected to be present were plotted on transparent film overlays using American Society for Testing and Materials (ASTM) card data. The scale of these overlays allowed the sample film to be placed directly over the transparency. Only patterns which could not be identified by this method were measured; detailed searches for their identities were performed in the ASTM powder diffraction file. Patterns that had too few lines to identify were listed as unknowns.

The electron microprobe was used to determine the elemental content of individual mineral grains and to study the phase relationships of the intergrowths. Analyses were performed using the Materials Analysis Company model 400 electron microprobe. Two crystal spectrometers were used so two elements could be analyzed simultaneously. One, equipped with a potassium acid phthlate (KAP) analyzing crystal and a gas flow proportional detector, was used for analyzing Mg, Al, and Si. The other, equipped with a lithium fluoride (LiF) crystal and a sealed proportional detector, was used for Cr, Fe, Ni, and Mn. Most analyses were performed using a 15 kilovolt accelerating potential. Standards of well-analyzed olivine and chromite were used to minimize matrix corrections for Si, Mg, Fe, Cr, Al, and Mn. Pure Ni was used for a Ni standard. Matrix effects (fluorescence, absorption, and atomic number) were corrected by a computer program using either *Albee's and Ray's* [1970] or *Sweatman's and Long's* [1969] procedures. Thin lamella-like intergrowths and small particles were analyzed using low KeV methods reported by *Cunningham et al.* [1972]. This method does not require matrix corrections. Qualitative analyses were obtained with an energy dispersive Li-drifted silicon detector for elements with atomic numbers of 12 or higher.

Scanning electron microscopy was used to supplement optical microscopy and to resolve textural and morphological features too small to be seen optically. A Joelco JSMU-3 scanning

electron microscope (SEM) was used for all electron microscopy. Since the SEM is equipped with an energy dispersive X-ray detector, qualitative elemental analyses of the small scale intergrowths were also performed.

Bulk chemical analyses to determine changes in bulk composition due to volatile depletion were performed by the Mineral Constitution Laboratories of Pennsylvania State University under the direction of J. B. Bodkin. The accuracy of these measurements was better than ±0.1% by weight for most elements.

EXPERIMENTAL RESULTS

Original olivine sample. The olivine sample consisted of 98% olivine (including traces of olivine alteration products) and 2% chromite. The olivine grains were generally rounded, equant shaped, and ranged in size from 0.2 to 2 mm (see Figure 2). The larger grains had extensive fractures. There was no evidence of zoning. An alteration product occurred along grain boundaries and fractures. The chromite grains were opaque and generally euhedral to subhedral shaped, and ranged in size from 0.1 to 2 mm.

The olivine composition was Fo-89 based on the d_{130} interplaner spacing [*Yoder and Sahama*, 1957], and Fo-91 based on the d_{062} interplaner spacing [*Hotz and Jackson*, 1963]. There was little variation in olivine composition as indicated by the sharp, narrow diffraction peaks. Electron microprobe scans across several grains detected no changes in Fe and Mg content. Hence, no zoning was present. Quantitative elemental microprobe analyses of several olivine grains are shown in Table 1. Calculation of the olivine formula from these data yields $(Mg_{1.83}\ Fe_{0.16}\ Ni_{0.01})\ SiO_4$ or Fo-91.5.

Quantitative microprobe analysis of olivine alteration products was not possible. Reactions occurred when the the sample was subjected to the electron beam. This result was attributed to

to the hydrous nature of the sample. Major amounts of Mg and Si were detected along with minor amounts of Fe and occasionally Ni. Talc and serpentine were finally identified from the bulk sample using X-ray diffraction. A pure sample could not be separated and the identification was complicated by low diffraction intensities and interfering olivine lines.

Quantitative elemental microprobe analyses of several chromite grains are shown in Table 1. Calculation of the chromite formula from these data yields $(Mg_{0.31}\ Fe_{0.69})\ (Cr_{1.52}\ Al_{0.48})O_4$. The cell dimension ($A_o$ = 8.321Å) calculated from the diffraction pattern was slightly smaller than for pure $FeCr_2O_4$ (A_o = 8.378Å). This observation is a result of partial substitution of Al^{+3} for Cr^{+3}, and Mg^{+2} for Fe^{+2} [*Deer et al.*, 1962].

Ablated olivine sample. The ablated olivine material has been divided into the following two groups: (1) debris composed of material formed in the ablation zone on the sample's front face (fusion crust) and the buildup of this matter into flanges and stringers along the outer margins of the sample (see Figure 1); and (2) individual particles smaller than 1,000 μ in size, having spherical to angular shapes. Since the ablated debris massing at the outer margins of the sample is quite fragile and frequently falls away, it may contribute significantly to the smaller sized individual particle population. Material along the sample's front face corresponds to the fusion crust of actual meteorites. The fragile matter and the small individual particles correspond to ablation debris collected in the atmosphere and at the earth's surface.

Debris from ablation zone and material forming flanges and stringers. The olivine was completely melted and recrystallized (see Figure 3). All hydrous olivine alteration products were destroyed. A new mineral, magnetite, was formed which exsolved from the original olivine (*Cunningham and Blanchard*, 1972; *Cunningham*, 1973). A few relict grains of chromite still existed. Vesicles were a common feature characterizing the debris. These were formed both by

the loss of volatiles from the sample and the interaction of the plasma with the ablating material. No glass was identified in thin sections.

The olivine composition, determined by X-ray diffraction methods, was Fo-94 based on the d_{130} spacing (*Yoder and Sahama*, 1957), and Fo-95 based on the d_{062} spacing (*Hotz and Jackson*, 1963). This composition represented about a 50% decrease of Fe in the recrystallized olivine. Electron microprobe analysis (Table 1) showed the recrystallized olivine had become enriched in Mg and depleted in Fe. No evidence of zoning was found from Fe/Mg ratios on scans across recrystallized olivine grains. However, differences in grain-to-grain composition were now common. Iron varied from 2.1 to >4.0%, and Mg varied from 32.7 – 31.0%. Recrystallized olivine grains near outer edges of flanges and stringers were usually more Fe deficient than those near the central portion.

Lamella-like intergrowths of magnetite in recrystallized olivine grains were prevalent constituents. Magnetite was positively identified by X-ray diffraction performed on an opaque fraction separated from the recrystallized olivine. While most of these intergrowths were only a few microns wide, some were 10 μ. Their lengths ranged (in a discontinuous fashion) from a few to 1,000 μ. Precise quantitative analysis was not possible on grains having this shape and size. However, semiquantitative data (Table 1) were obtained employing low KeV analysis techniques [*Cunningham et al.*, 1972]. The low KeV method insures the volume analyzed by the electron beam will be a minimum size. Results showed compositions were quite variable for these intergrowths. The Fe + Cr content ranged from 36.0 to 62.2%, with Fe being 24.5 to 54.6% and Cr being 1.3 to 15.2%. The content of both Si and Mg was occasionally as high as 12%. Usually the Fe + Cr content was inversely related to the Mg + Si. Since only a small amount of Si can be accommodated within the magnetite structure, most of the Si and Mg was from the olivine matrix.

Wherever magnetite occurred, there was a corresponding decrease of Fe in the recrystallized olivine. This finding proved the magnetite was formed during partial oxidation of Fe from the olivine grain. To determine if Si was also released from the olivine during the formation of magnetite, a microprobe scan was performed across an olivine grain containing magnetite intergrowths (Figure 4). Results showed the Si content at the edges of these intergrowths sometimes increased with an increase in Fe, and sometimes decreased with an increase in Fe. Scanning electron microscopy images taken of a magnetite intergrowth having a high Si content at its margins (Figure 5) revealed myrmekitic-like intergrown phases. Qualitative X-ray analysis of these phases with the SEM showed the light colored phase was rich in Fe (and sometimes Cr) and deficient in Si and Mg. In contrast, the dark colored phase was rich in Si and relatively depleted in Fe. Hence, the borders of the lamella-like magnetite intergrowths were surrounded by myrmekitic-like intergrown phases of Cr-rich magnetite and a Si-rich phase (probably amorphous).

Some chromite grains passed through the ablation process without being completely destroyed. These relict chromite grains exhibited reaction rims. Scanning electron microscopy images of these reaction rims (Figure 6) again showed myrmekitic-like intergrown phases. The light phases were rich in Fe and the dark phases rich in Si. It was shown by the X-ray diffraction of separated grains that the relict grains were the same chromite as that in the original sample. This observation means that the chromite was not molten long enough for all of it to react with the olivine melt and diffuse into the newly formed magnetite.

Bulk chemical analyses, shown in Table 2, revealed only minor changes in overall composition. The only significant constituent depleted during ablation was water. Sources for the water were the hydrated minerals which were destroyed in the process. Small increases for

SiO_2 and MgO are probably real. Small decreases for the other oxides are so close to the analytical error that they should not be considered real.

The fusion crust (Figure 7) can be divided into four zones. In the first zone, the sample shows no ablation effects. In the second zone (typically 50 μ thick), the principal effect is due to heat. This effect is clearly indicated by olivine discoloration and a corresponding destruction of hydrated minerals. There is no evidence of melting in this zone. In the third zone (typically 50 μ thick), the initial reactions take place. Discontinuous and irregular intergrowths and occasional globules of exsolved magnetite develop along grain boundaries and along the grain face exposed to the beam. Often the integrity of the original olivine grain has been retained throughout, indicating complete melting did not occur. Evidence of this incomplete melting is shown by the appearance of olivine grains when viewed under cross-polarized light. The optical orientation of the olivine grain is identical to that of the unaltered portion. Continuation of fractures through this zone is also evidence indicating incomplete melting has occurred. Electron microprobe analyses of the olivine adjacent to the exsolved magnetite indicates Fe was depleted. This zone exhibits features common to both solid-state diffusion and incongruent melting. The Fe is being concentrated in newly formed, irregular intergrowths and globules of magnetite and, at the same time, the Mg is being concentrated into the remaining olivine. The fourth zone is often absent, but when present, consists of completely recrystallized olivine and lamella-like intergrowths of magnetite. These intergrowths are 20–50 μ apart and less than 10 μ wide, and are oriented in a pattern more-or-less parallel to the long axis of the recrystallized olivine grain. This material was identical to that found in the debris which was located along the outer margins of the sample and formed flanges and stringers. This melted and recrystallized portion of the fusion crust is discontinuous and typically 100 μ thick. Evidence indicates the molten material flows rapidly away from the sample's face due to aerodynamic forces of the high velocity plasma.

Individual particles smaller than 1000 μ. Particles smaller than 1000 μ were recovered from the copper collector and divided into morphologic groups. Five percent (by weight) of these particles showed no evidence of melting. Twenty-four percent (by weight) were spherules formed by melting. The rest consisted of shapes exhibiting melt features. This evidence indicates ablation debris may be expected to exhibit a wide variation in morphologic characteristics.

A representative sample from each of these groups of particles was selected for X-ray diffraction. A total of 98 particles were analyzed. The results are given in Table 3. Olivine and magnetite were the most common minerals, with magnetite always occurring as a minor constituent. Since magnetite was a minor constituent, it was recognized in only 14% of the diffraction patterns. However, the lamella-like intergrowths probably occur in all particles because they were observed in every particle prepared for polished sections. Five of the olivine particles also contained other diffraction lines which could not be identified. There were five patterns for which no mineral identifications could be made. The one quartz particle identified was probably a contaminant rather than an ablation product. The copper particles were contaminants from the collector. Particles were listed as amorphous if no diffraction pattern was obtained after two or more separate exposures.

Electron microprobe analysis was performed on eight particles under 300 μ in size (see Figure 8). Elemental content in these spheres is shown in Table 4. The olivine composition is nearly the same as the other ablation debris (see Table 1). Submicroscopic magnetite (or chromite) probably accounts for the Al and high Fe content in spherules E and H. Quantitative analyses of these magnetite intergrowths was not possible because of their small size. Glass was not observed except on the thin edges of those particles which were rapidly quenched when striking the collector.

DISCUSSION

Olivine ablation regime. The olivine ablation regime is one of rapid heating with melting and vaporization of the sample. For these experiments, a high temperature (≈11,000°K) plasma gas cap forms behind the bow shockwave at the ablating face and produces an oxidizing environment. The resultant molten material and vapors are continuously swept away by aerodynamic forces. The material is swept away into the free stream (≈1,500°K) and cools at rates which are dependent upon the size of the individual particles. For small particles, extremely rapid cooling occurs since spheres are solidified before striking the collector less than 2 ft away from the ablating sample. The environment during cooling is less oxidizing than at the ablating face. Physical and thermal shock occur in the sample, as is evidenced by fracturing and production of unmelted debris. Both cooling and solidification are too rapid for equilibrium conditions to develop. Rapid changes in composition are common. The characteristics of ablation debris are the result of these conditions and must be interpreted within such a framework.

As the sample is heated, the first effects are discoloration and loss of water from low temperature hydrated minerals. With continued heating, the olivine begins to oxidize, forming thin lamella-like intergrowths of magnetite oriented parallel to the olivine crystallographic planes. Surrounding these intergrowths are myrmekitic-like intergrown phases of magnetite and a silica-rich phase. This structure is believed to result from both solid-state diffusion and incongruent melting. Diffusion of Fe to the intergrowths and complementary diffusion of Mg to replace it occurs. Excess Si from olivine forms the silica-rich phase. The olivine is enriched in Mg and depleted in Fe. The melt rapidly flows away, leaving the ablation face with only a thin crust of melted material. The melted debris rapidly recrystallizes after its removal from the ablation zone. However, no glass is formed in the debris. Magnetite intergrowths remain with their orientation controlled by the olivine structure. Olivine in the inner portion of the large

recrystallized debris has a higher iron content than that at the surface. This composition is a result of the continued oxidation of the olivine at the surface. The ablated debris has numerous vesicles produced from volatile elements in the sample as well as air trapped from the plasma.

Comparison with earlier work. The olivine ablation experiment has many features in common with previous iron oxide experiments. Textural and morphological characteristics are indicative of the ablation environment. Most of the debris has melted, forming new and recrystallized minerals. Fine intergrowths of dissimilar amorphous and crystalline phases were abundant. Individual particles in the $<1{,}000\ \mu$ size range included spherules as well as angular-shaped grains showing no signs of having been melted. Volatile depletion occurred. For olivine, this process consisted of the depletion of water from hydrated minerals which were destroyed in the process. In the case of the iron oxides, P and Cl were depleted by about 50%, while lesser amounts of Si and Ca were lost.

A significant amount of Fe from the olivine was oxidized during ablation. This result had been predicted based on earlier laboratory experiments. *Bowen and Schairer* [1935] observed incongruent melting of silicates with separation of iron while studying the $MgO\text{-}FeO\text{-}SiO_2$ system. More recently, *Champness* [1970] produced iron oxides, olivine, and silica from olivine powder which was heated in air for several hours below melting temperatures. In these experiments, the silica was often amorphous, but sometimes occurred as cristobalite or tridymite. Diffusion of Fe to the nucleation zone of the iron oxides and complementary diffusion of Mg to replace the Fe occurred. This last feature is similar to the current experimental observations where oxidation of olivine formed the magnetite intergrowths in the ablation zone. However, no pyroxene or cristobalite (or tridymite) was produced in these ablation experiments because the time was too short for equilibrium to occur.

The formation of magnetite in the fusion crusts of meteorites has been previously observed. *Ramdohr* [1967] discussed the mineralogy and the appearance of fusion crusts of many meteorites; he also described a spinel-structured mineral often occurring in the outer portions of the fusion crust where oxidation was greatest. On the basis of reflected light microscopy, he identified it as magnesioferrite ($MgOFe_2O_3$). *Florenskiy et al.* [1968] found magnetite and Mg-rich magnetite (Magnesium-magnetite) in silicate spheres from ablation material collected from the Tunguska meteorite fall. More recently, *Florenskiy and Ivanov* [1972] have described the melting of meteoritic ferrous silicates as incongruent decompositions into magnetic and silicate phases, with their subsequent separation. Based on data in this paper, the formation of magnetite from olivine during ablation appeared to be both by solid state diffusion and incongruent melting.

Comparison with Allende and Murchison meteorite fusion crusts. Results of the olivine ablation study suggested that the formation of magnetite intergrowths and a corresponding Fe depletion and Mg enrichment in the recrystallized olivine were characteristic of ablation debris from meteoritic olivine. This hypothesis was tested by examining fusion crusts from Allende and Murchison chondritic meteorites. A thin section from the Allende (C3 carbonaceous chondrite) meteorite was provided by D. Brownlee, University of Washington. While the Allende fusion crust had been reported to be a dense opaque glass [*Clarke et al.*, 1970], very little glass was found in this thin section. Ultrathin sections (1−5 μ thick) revealed numerous opaque micron-sized inclusions in a micro-crystalline matrix (see Figure 9). The results of X-ray diffraction studies of samples from the original meteorite confirmed the composition of the olivine matrix was near Fo-50. In contrast, X-ray diffraction showed the fusion crust contained an olivine with a higher Fo content and magnetite. Energy dispersive X-ray analysis of the fusion crust with the SEM confirmed the opaque grains as magnetite and the transparent grains as an olivine, more

Mg-rich and Fe-deficient than the original meteorite matrix. Studies of the Murchison meteorite fusion crust (C2 carbonaceous chondrite) by X-ray diffraction revealed similar magnetite grains in an olivine ground mass, even though the original meteorite had principally a chamosite matrix. A more detailed discussion of these analyses has been reported (D. E. Brownlee, R. Beauchamp, G. Cunningham, and M. B. Blanchard, unpublished data, 1973).

CONCLUSIONS

Identification criteria for ablation debris from olivine. The melting and oxidation of olivine during meteor ablation, producing magnetite and an Fe-deficient olivine, is indicative of the ablation environment and may be used as criteria for the identification of ablation debris. The close intergrowth of magnetite in olivine grains is clear evidence of oxidation during the rapid ablation process. Loss of volatile components, destruction of low temperature hydrated minerals, formation of new minerals, and evidence of melting (i.e., shape and vesicles) are further criteria for ablation origin. Future samples collected from meteor and fireball trains should be studied to identify magnetite intergrowths in olivine spherules. An estimate of the original composition of a meteorite from only ablated material is presently possible for the nonvolatile constituents. Continued studies of other ablated minerals and meteorites will make inferences more accurate.

Acknowledgments. We wish to express our gratitude for assistance rendered by the LFE-Trapelo West staff (especially H. Lem-SEM) at Ames Research Center for support services under Contract NAS2-6006. Sincerest appreciation is expressed to W. C. A. Carlson and W. Winovich of the Ames High Enthalpy Research Branch for assistance in making the supersonic arc jet facility available for these experiments. A special thanks to Donald E. Brownlee, Astronomy Department, University of Washington, for his helpful discussions and for making the samples of the Allende and Murchison meteorite fusion crusts available.

REFERENCES

Albee, A. L., and L. Ray, Correction factors for electron probe microanalysis of silicates, oxides, carbonates, phosphates, and sulfates, *Anal. Chem.*, *42*, 1408–1414, 1970.

Blanchard, M. B., Preliminary results of artificial meteor ablation, *Meteoritics*, *4*, 261–262, 1969.

Blanchard, M. B., Artificial meteor ablation studies of iron oxide minerals, *Eos Trans. AGU*, *51*, 831, 1970a.

Blanchard, M. B., Wustite, a common occurrence in artificial meteor ablation products, *Meteoritics*, *5*, 181–182, 1970b.

Blanchard, M. B., Artificial meteor ablation studies: iron oxides, *J. Geophys. Res.*, *77*, 2442–2455, 1972.

Blanchard, M. B., and G. G. Cunningham, Preliminary results of artificial meteor ablation of an olivine mineral sample, *Meteoritics*, *8*, 15, 1973.

Brownlee, D. E., and P. W. Hodge, Results of a large volume micrometeorite collection at an altitude of 115,000 feet, *Meteoritics*, *4*, 264–265, 1969.

Bowen, N. L., and J. F. Schairer, The system MgO-FeO-SiO_2, *Amer. Jour. Sci.*, *29*, 151–217, 1935.

Carr, M. H., Atmospheric collection of debris from the Revelstoke and Allende fireballs, *Geochim. Cosmochim. Acta*, *34*, 689–700, 1970.

Champness, P. E., Nucleation and growth of iron oxides in olivines, *Mineral. Mag., 37,* 790–800, 1970.

Clarke, R. S., E. Jarosewich, B. Mason, J. Nelen, M. Gomez, and J. R. Hyde, The Allende, Mexico, meteorite shower, *Smithsonian Contrib. Earth Sci., 5,* 53 pp., 1970.

Cunningham, Gary G., Ablation studies of an artificial meteor of olivine composition, M.S. thesis, Geology Dept., Calif. State Univ., San Jose, 59 pp., 1973.

Cunningham, Gary G., and M. B. Blanchard, Magnetite, a common occurrence in artificially ablated olivine samples, *Eos Trans. AGU, 53,* 1036, 1972.

Cunningham, G. G., T. D. Palmer, K. G. Snetsinger, and M. B. Blanchard, Low kev electron probe analysis of silicate minerals Mg, Al, and Si using pure-element standards, *Proceedings Seventh National Conference of the Electron Probe Analysis Society of America, 53A–53C,* San Francisco, Calif, July, 1972.

Deer, W. A., R. A. Howie, and J. Zussman, *Rock forming minerals,* vol. 5, *Non-silicates,* 371 pp., Longmans, Green and Co., LTD., London, England, 1962.

Finkleman, R. B., Relationship between manganese nodules and cosmic spherules, *Mar. Technol. J., 6,* 34–39, 1972.

Florenskiy, K. P., and A. V. Ivanov, Differentiation of meteoritic matter in the Earth's atmosphere, *NASA Tech. Translation TT F-14,138,* 17 pp. From *Meteoritika, 30,* 104–113, 1970.

Florenskiy, K. P., A. V. Ivanov, O. A. Koriva, and N. I. Zaslavskaya, Phase composition of the extraterrestrial dust in the region of the Tunguska fall, *Geochem. Int., 5,* 977–984, 1968.

Hotz, P. E., and E. D. Jackson, X-Ray determinative curve for olivines of composition Fo_{80-95} from stratiform and alpine-type periodotites, *U.S. Geol. Surv. Prof. Paper, 450E*, E101–E102, 1963.

Kornblum, J. J., Micrometeoroid interactions with the atmosphere, *J. Geophys. Res., 74*, 1893–1970, 1969.

Ramdohr, P., Die schmelzkruste der meteoriten, *Earth and Planetary Sci. Lett., 2*, 197–209, 1967.

Shepard, C. E., J. W. Vorreiter, H. A. Stine, and W. I. Winouich, A study of artificial meteors as ablators, *NASA Tech. Note D3470*, 33 pp. 1967.

Sweatman, R. R., and J. V. P. Long, Quantitative electron probe microanalysis of rock-forming minerals, *J. Petrol. 10*, 332–379, 1969.

Yoder, H. S., and T. G. Sahama, Olivine X-ray determinative curve, *Amer. Mineral. 42*, 475–491, 1957.

TABLE 1. Electron microprobe analyses of original olivine sample and ablated olivine sample

Mineral Constituents	Element	Weight Percent	
		Original	Ablated
Olivine	Fe	6.09±0.10	2.95*
	Mg	29.87±0.32	32.09
	Si	18.88±0.08	19.64
	Ni	0.20±0.02	0.18
	O‡	44.96	45.14
Chromite	Al	5.96±0.09	5.25±0.09
	Fe	21.79±0.26	21.95±0.26
	Cr	36.51±0.32	38.64±0.34
	Mg	4.28±0.15	3.89±0.14
	O‡	31.46	30.27
Magnetite	Fe		30.71–57.77†
	Cr		0.33–18.78
	Si		1.37–12.15
	Mg		2.16–12.06

*Values for ablated olivine are averages of analyses of five different grains.

†Values for magnetite ablated are the range of compositions measured.

‡Values for oxygen were obtained by subtraction.

TABLE 2. Bulk elemental composition of olivine sample and ablated olivine sample; data are based on wet chemical analyses

Oxide	Weight Percent	
	Original	Ablated
SiO_2	39.66	40.90
Fe_2O_3	<0.01	1.91
	9.15*	9.22*
FeO	8.23	6.57
MgO	48.62	49.47
Al_2O_3	0.16	0.20
TiO_2	<0.01	<0.01
Cr_2O_3	0.92	0.79
MnO	0.13	0.13
CaO	0.23	0.19
Na_2O	<0.01	<0.01
K_2O	<0.01	<0.01
NiO	0.28	0.25
Total H_2O	1.31	0.02
Total	99.53	100.43

*Total Fe expressed as Fe_2O_3.

TABLE 3. X-ray diffraction analysis of ablated particles

Minerals Identified	Frequency of Occurrence, %	
	Major	Minor
Olivine	82	
Magnetite		14
Quartz	1	
Copper	5	
Amorphous	5	
Unknown	5	5

TABLE 4. Microprobe analyses of ablated olivine spheres; values are given in weight percent

Sphere	Mg	Si	Al	Cr	Fe	Ni
A	31.82	19.56	N.D.*	0.07	2.05	0.16
D	30.90	19.02	N.D.	0.27	2.32	0.18
E	29.11	19.05	0.11	0.56	5.87	0.19
F	31.02	19.07	N.D.	0.41	2.88	0.20
G	31.92	19.46	N.D.	0.29	2.53	0.17
H	31.50	19.54	0.03	0.27	7.41	0.16
I	32.13	19.47	N.D.	0.22	2.61	0.20
Z_4	31.52	18.45	N.D.	0.16	2.27	0.18

*N.D. – Not detected.

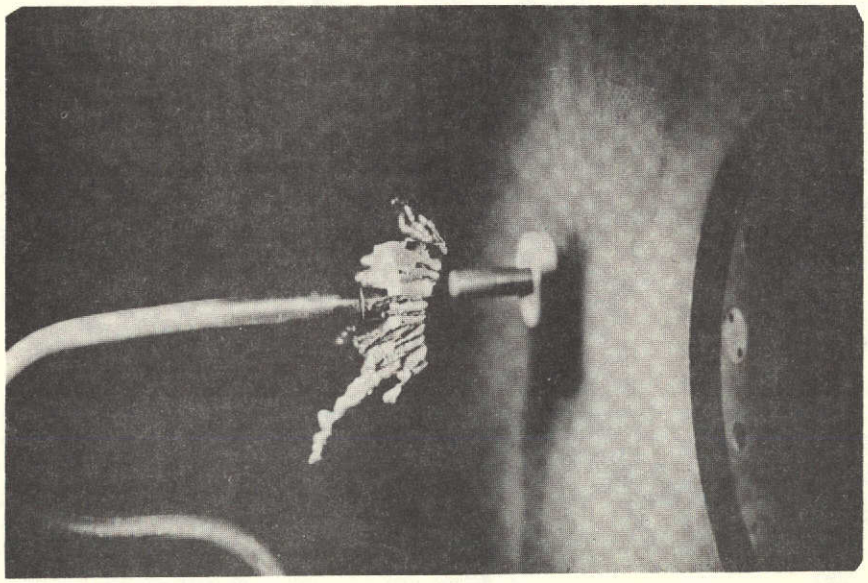

Fig. 1. Olivine sample mounted on copper stang in constricted-arc supersonic jet facility after ablation experiment.

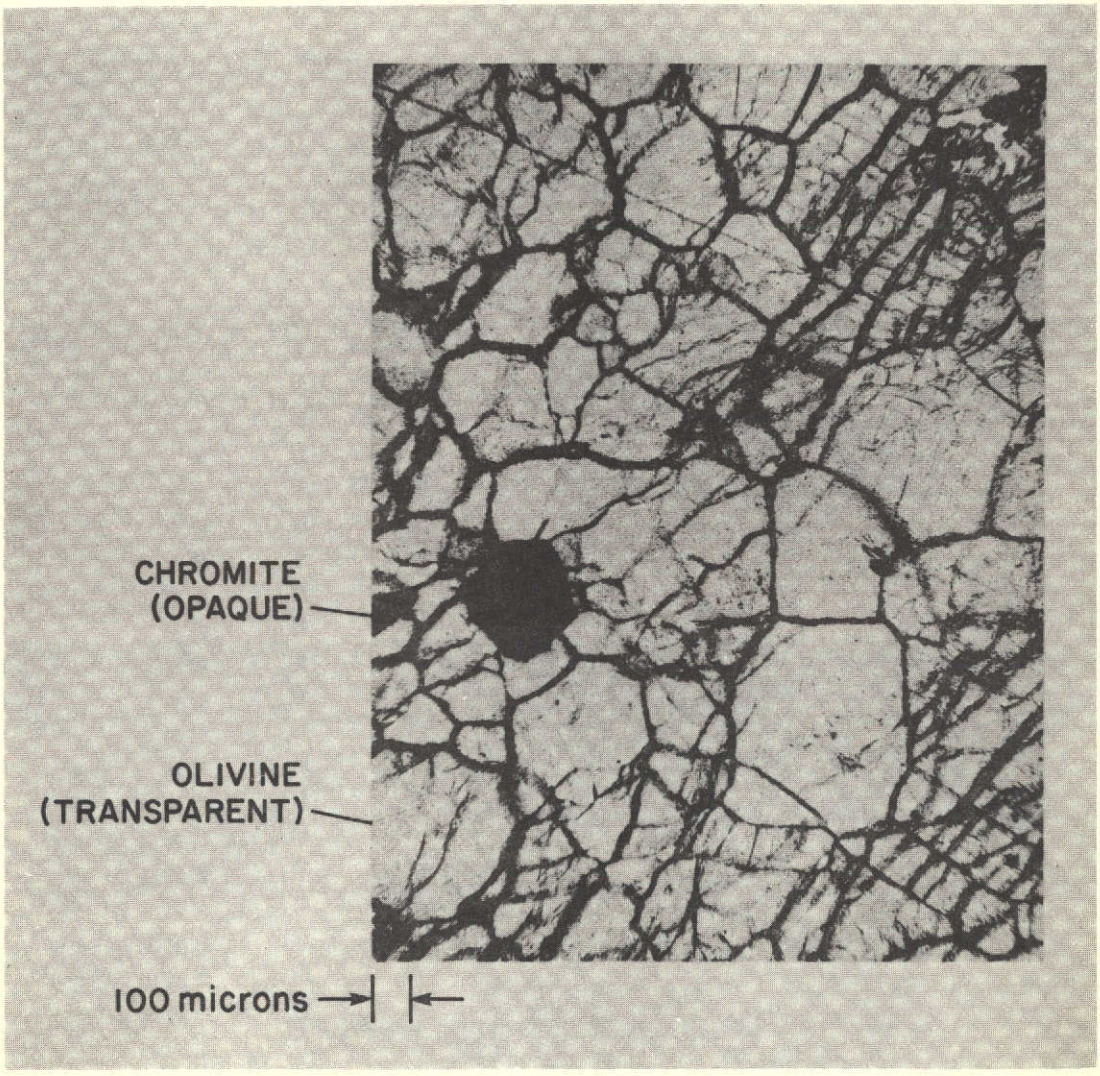

Fig. 2. Photomicrograph of thin-section from original olivine sample taken in plane polarized light.

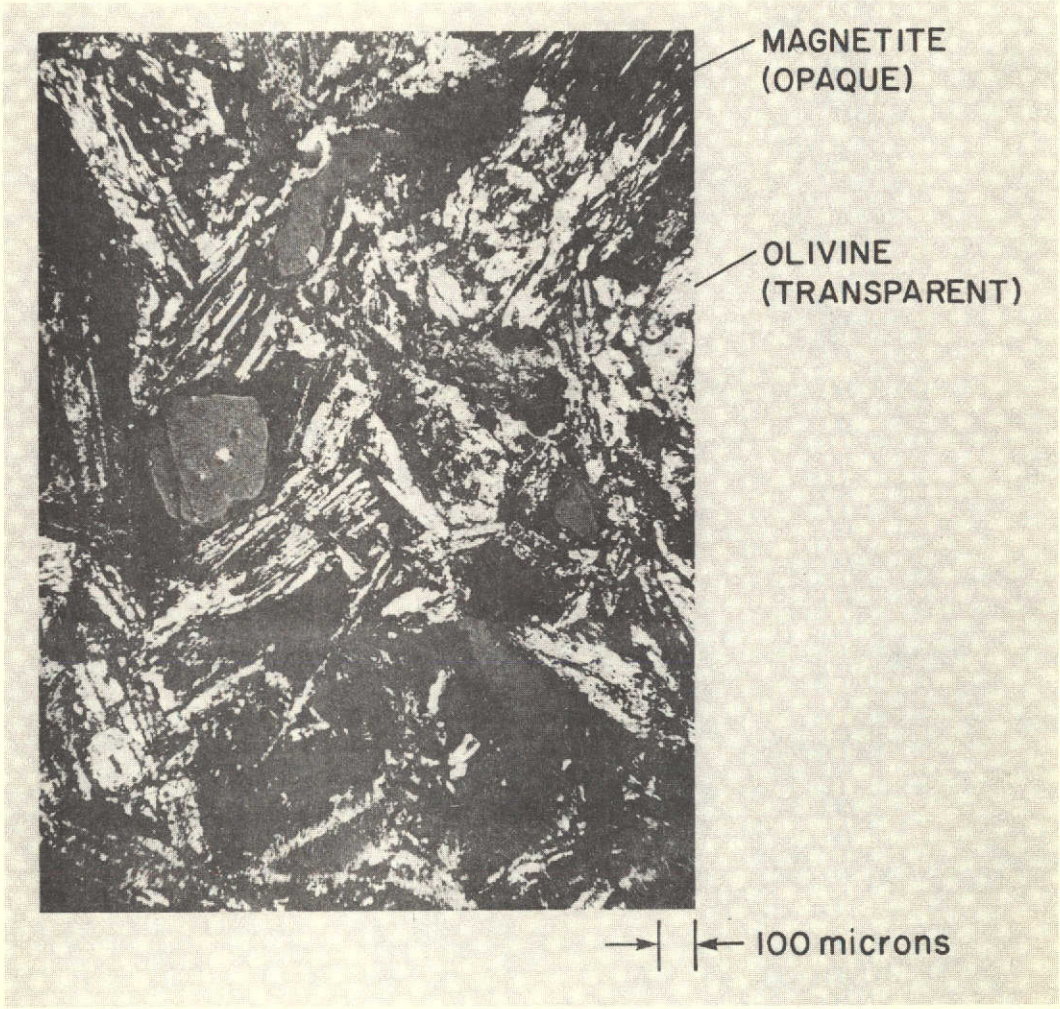

Fig. 3. Photomicrograph of thin-section from ablated olivine sample taken in plane polarized light.

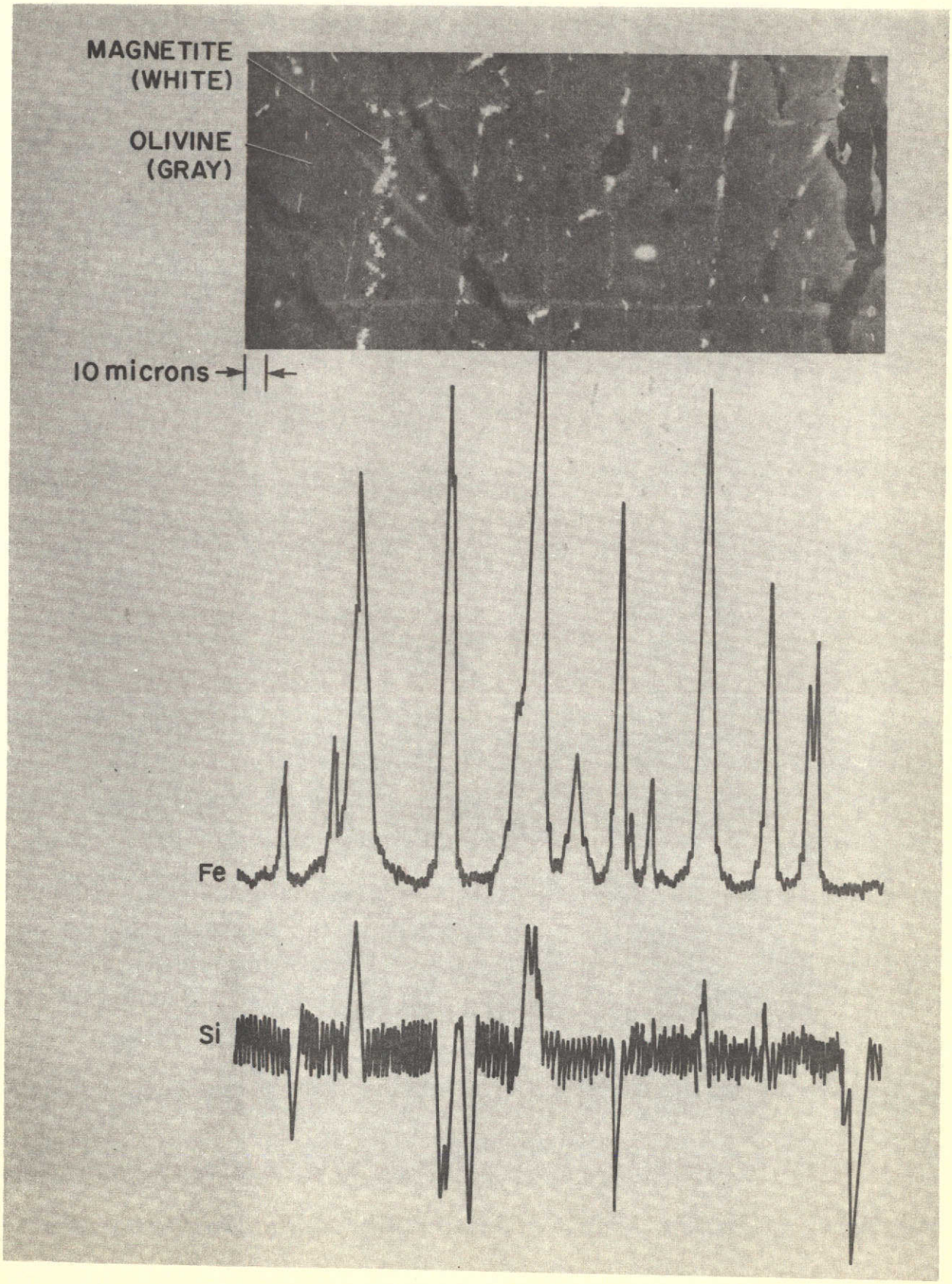

Fig. 4. Electron microprobe traverse along A–B in ablated olivine sample with spectrometers set to detect Fe and Si.

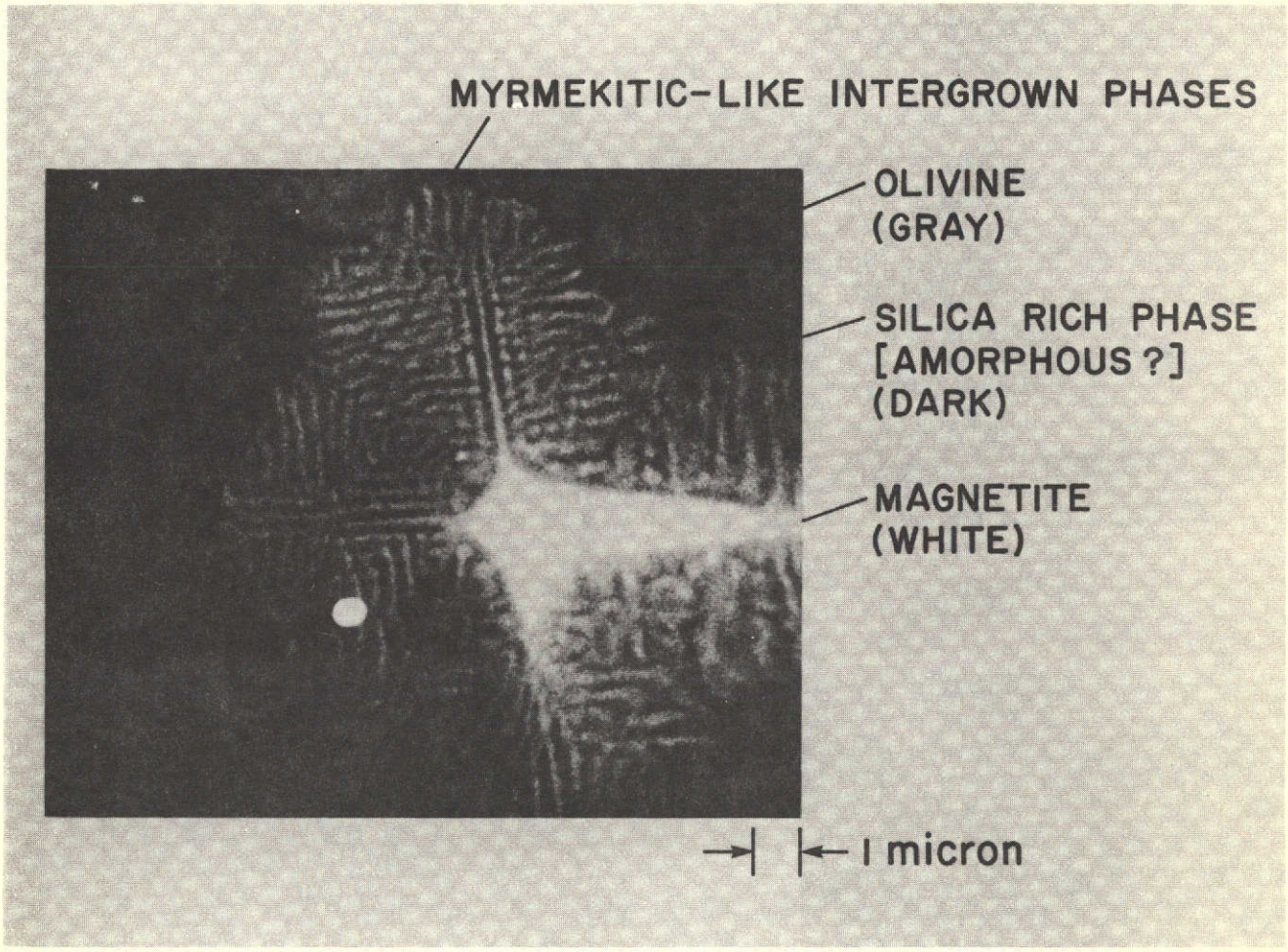

Fig. 5. Secondary electron image taken with SEM of magnetite intergrowths in ablated recrystallized olivine (light areas have high Z and dark areas have low Z).

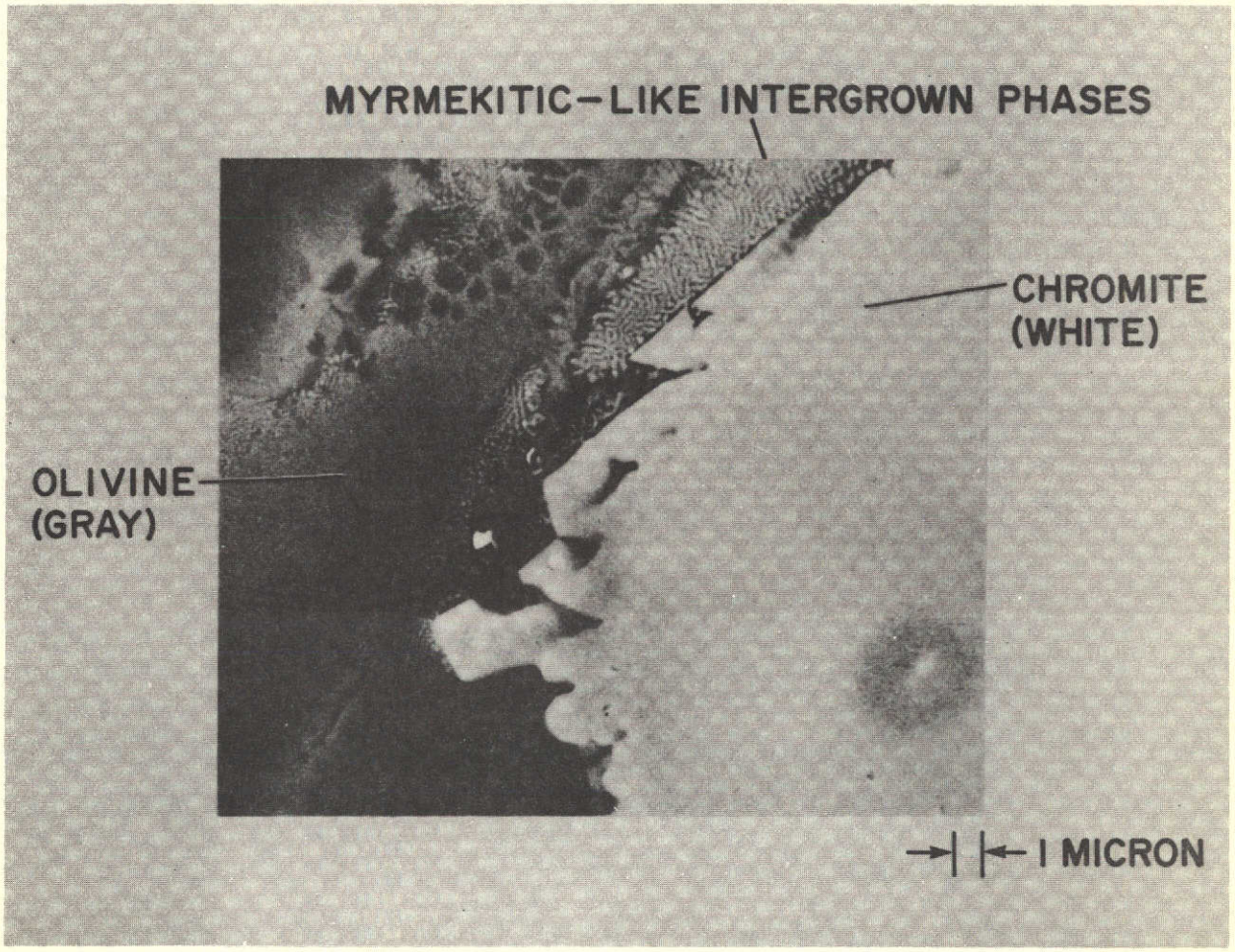

Fig. 6. Secondary electron image taken with SEM of reaction rim around chromite grain (light areas have high Z and dark areas have low Z).

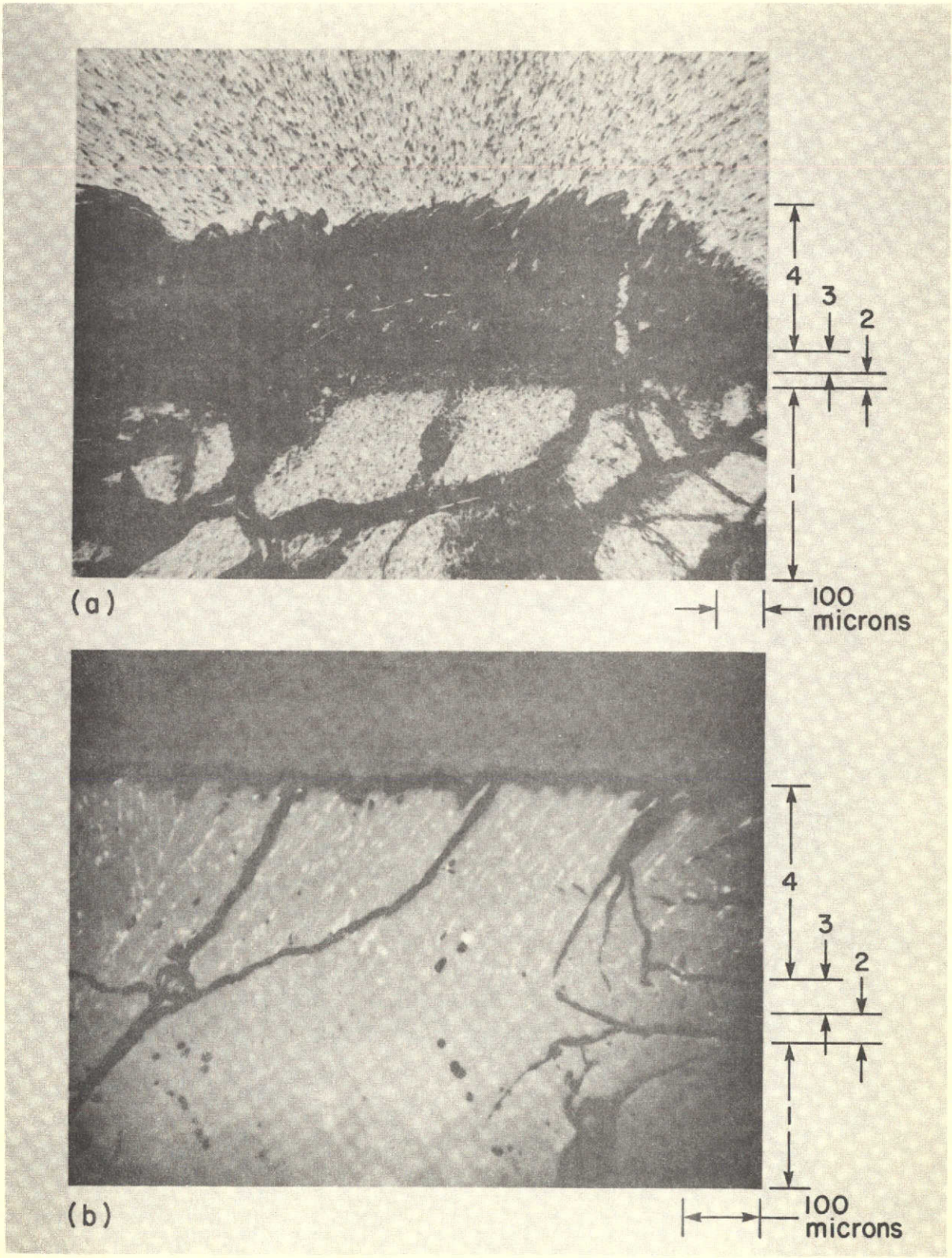

Fig. 7. Photomicrograph of thin-section (A) and polished section (B) of fusion crust in ablation zone along front face of olivine sample. Labeled zones: (1) unaltered olivine; (2) discoloration by heat; (3) transition where magnetite intergrowths form; and (4) complete melting and recrystallization of olivine.

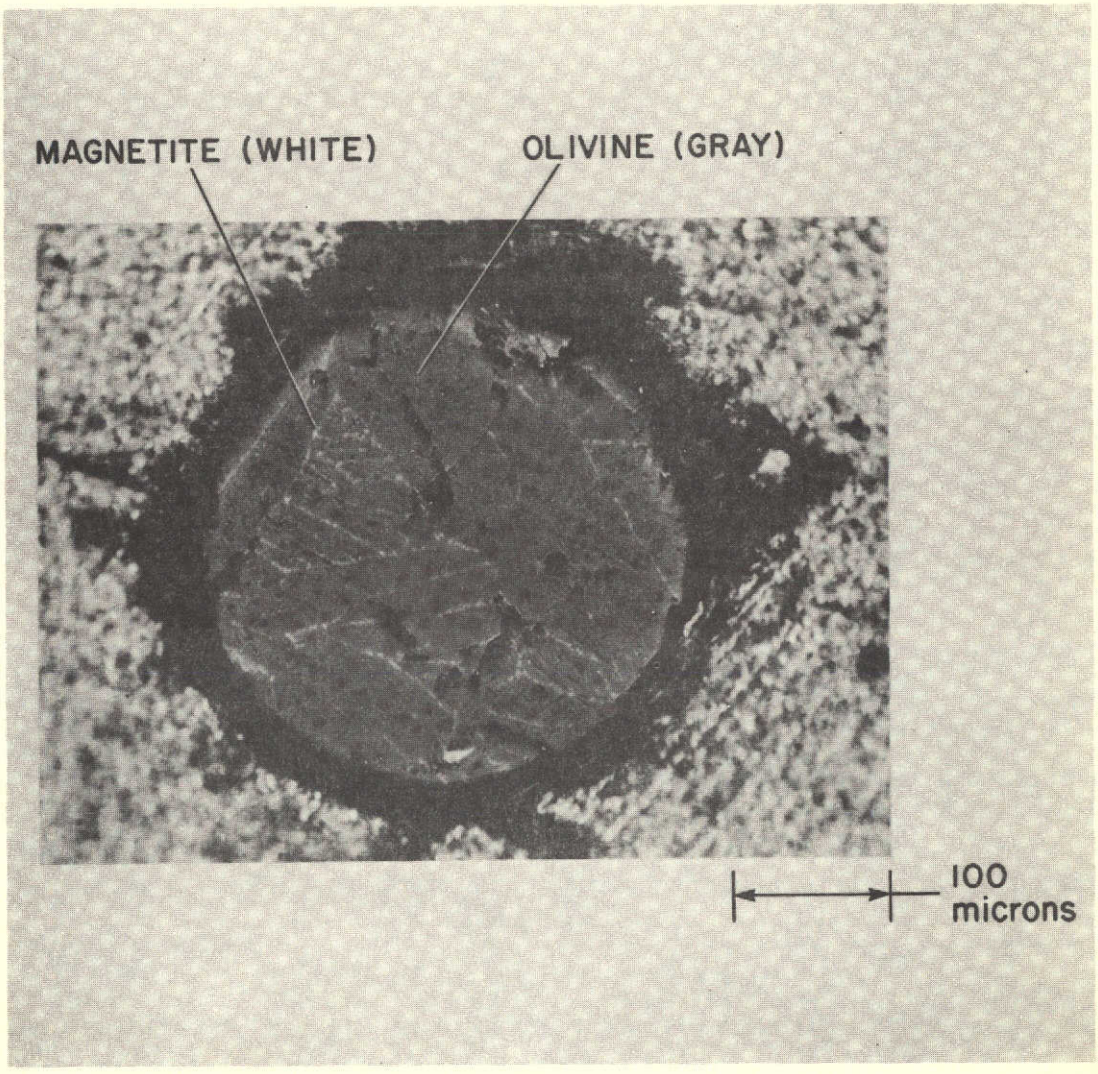

Fig. 8. Photomicrograph of polished section from olivine spherule.

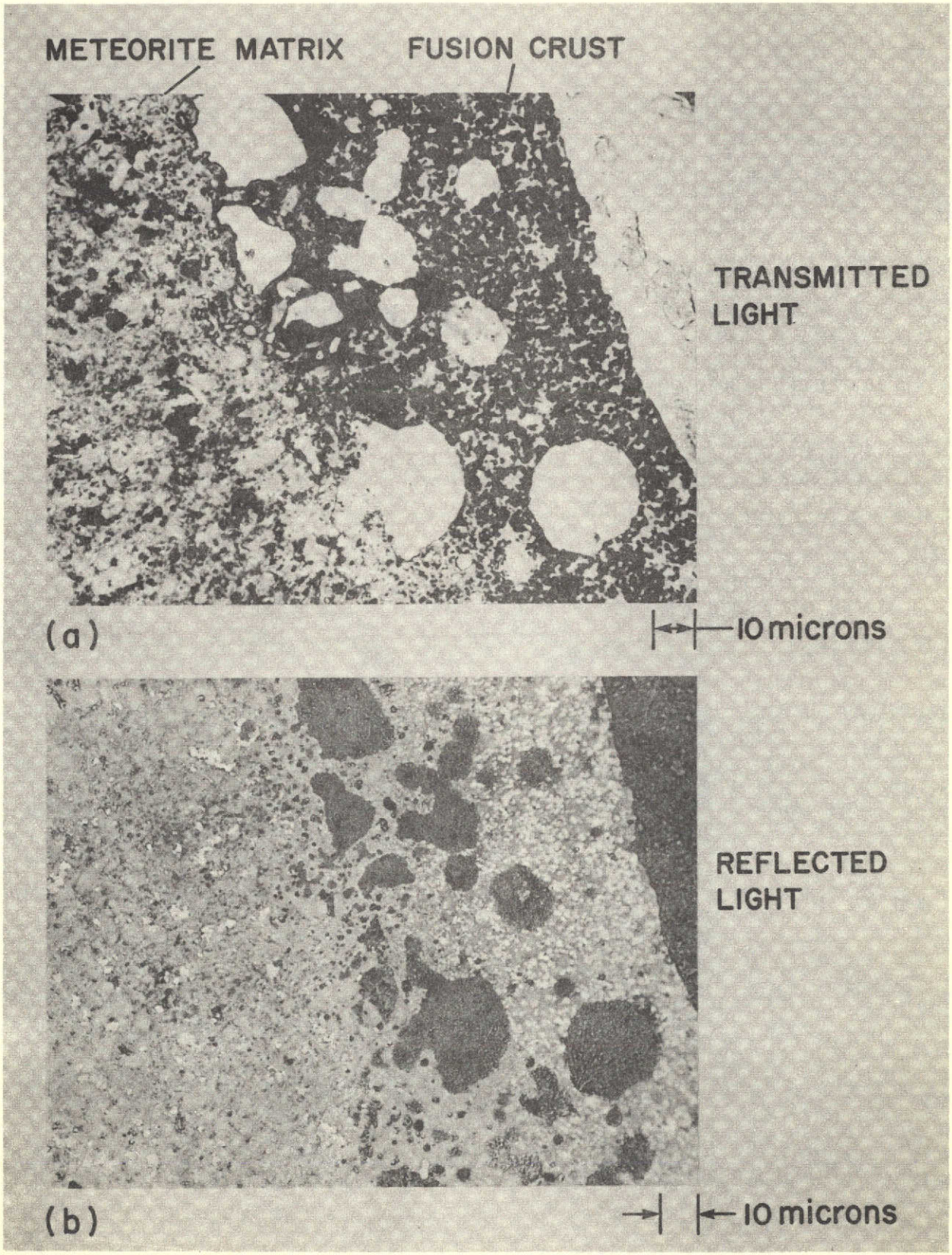

Fig. 9. Photomicrograph of Allende meteorite fusion crust showing newly formed magnetite.